Inhibition of Vascularization in Tumor Growth

M. Scalerandi[1] and B. Capogrosso Sansone[1,2]
[1]*INFM, Dipartimento Fisica, Politecnico di Torino, Torino, Italy*
[2]*Los Alamos National Laboratory, Los Alamos, New Mexico*
(Received 21 March 2002; revised manuscript received 10 September 2002; published 1 November 2002)

The transition to a vascular phase is a prerequisite for fast tumor growth. During the avascular phase, the neoplasm feeds only from the (relatively few) existing nearby blood vessels. During angiogenesis, the number of capillaries surrounding and infiltrating the tumor increases dramatically. A model which includes physical and biological mechanisms of the interactions between the tumor and vascular growth describes the avascular-vascular transition. Numerical results agree with clinical observations and predict the influence of therapies aiming to inhibit the transition.

DOI: 10.1103/PhysRevLett.89.218101 PACS numbers: 87.17.Aa, 05.45.–a, 87.18.–h

Competition for nutrients is critical for the dynamics of neoplasms, since the availability of enough nutrients is essential for cancer cell proliferation and, consequently, for tumor growth. In a very initial phase (the avascular "phase"), solid tumors usually show, even *in vivo*, a certain degree of regularity, assuming an approximate spherical shape. At this stage, nutrients are provided by the existing vascular system, i.e., by capillaries located outside the region occupied by the tumor, and, due to their limited number, soon limit tumor growth. Experimental observations indicate that, during this phase, neoplasms grow up to a radius of a few mm and then stop growing [1]. Sometimes a transition to a new growth regime then occurs (the vascular phase): Starving tumor cells release a molecular messenger, generally called tumor angiogenetic factor (TAF), which induces vessel proliferation and the formation of a new net of capillaries which often infiltrate the tumor mass (angiogenesis) [2]. The tumor, now well fed, resumes its fast growth.

Intense experimental activity focuses on the development and optimization of therapies to inhibit vascularization by using antiangiogenic drugs [3–5]. Such an approach has advantages with respect to traditional anticancer therapies: Endothelial cells (ECs) are expected to be less efficient than cancer cells to acquire drug resistance and the molecules which act as angiogenesis inhibitors are more specific than normal chemotherapies.

A mathematical model, capable of describing the main features of the transition from avascular to vascular tumors, may help optimize such new therapies, be used for preliminary testing of different experimental protocols, and to suggest new approaches. Several models have described either the growth of avascular tumors [6–11] or angiogenesis [12,13], but, to our knowledge, none have treated the interactions between the growing tumor and the growing vasculature. We present a model which combines tumor growth and angiogenesis and compare a few model predictions with clinical observations.

Although the problem is complex, a few basic physical and biological properties provide a simple model. We consider a piece of tissue and discretize it into identical elements (each represented by a node $\vec{i}$). In each element, we define at each time t (also discretized) a concentration $c^t_{\vec{i}}(l)$ of cells of different types (l being the types index). To properly model the system, we have to consider at least six types: cancer, necrotic, and healthy cells ($l = 1, 2, 3$), and three types of ECs. As we showed in a recent paper [13], a model of angiogenesis must take into account vessel-forming ECs ($l = 4$), migrating ECs ($l = 5$), and fixed ECs structured in the shape of closed tubes ($l = 6$). Also, in each element we define the concentrations $n^t_{\vec{i}}(l)$ of molecules ($l = 1, 2$ are the indices for nutrient and TAF molecules). In the following, we will omit the indices whenever referring to the current time and node.

Cell behavior.—From a physical point of view, we consider cells as particles which exchange energy with the environment [8,14]. As such, they eventually accumulate an internal energy $b(l)$ (i.e., the energy of the absorbed molecules) which evolves according to an energy conservation rule:

$$b(l) \rightarrow b(l) + \gamma(l) - \beta(l) - kb(l), \tag{1}$$

where $\gamma(l)$ is the absorbed energy [proportional to the nutrient concentration per cell $n(1)/\sum_l c(l)$], and k is a coefficient of chemical energy release. $\beta(l)$ is the energy consumed by cell metabolism:

$$\beta(l) = \beta_0(l) + \beta_1(l) \exp[-\chi(l)A(l)], \tag{2}$$

The first term is constant (the so-called basal metabolic rate), while the amount $A(l)$ of absorbed signal molecules modulates the second [$\chi(l)$ is the cell sensitivity to the signal]. In particular, we consider here only the effect of TAFs on endothelial cells. Therefore, $\beta_1(l) = 0$ for $l = 1$–3 and $A(l)$ is proportional to the local TAF concentration per cell:

$$A(l) = \zeta(l) n(2) \Big/ \sum_{l=4}^{6} c(l). \tag{3}$$

Here $\zeta(l)$ measures the up-regulation of metabolism by TAFs. Cells absorb both nutrients and signal, with

$W(1) = \sum_l \gamma(l)c(l)$ and $W(2) = \sum_{l=4}^{6} A(l)c(l)$ being the amount of absorbed nutrient and signal, respectively.

We consider the internal energy to dictate the cell behavior [14,15]: If, for any types, the internal energy falls below a given threshold $[b_A(l)]$, some cells die of starvation at a rate R_A: $c(l) \rightarrow c(l)(1 - R_A)$. If the internal energy is larger than the mitosis threshold $[b_M(l)]$, cellular duplication occurs at a rate R_M:$c(l) \rightarrow c(l)(1 + R_M)$. Mitosis consumes part of the internal energy with the remainder split equally between daughter cells. Daughter ECs always belong to the free ECs types. The cells otherwise are in a latent state.

In addition, spontaneous cell death may be easily included. However, its effects are equivalent to the ones obtained by changing the starvation and mitosis rates.

Nutrient and signal evolution.—Nutrients and signal concentrations obey a reaction-diffusion equation with nonstationary sources and sinks:

$$n(l) \rightarrow [1 - \xi(l)]n(l) + \alpha_n(l) \sum_{\vec{n}} [n_{\vec{n}}(l) - n(l)] + S(l) - W(l), \quad (4)$$

where $\xi(l)$ and $\alpha_n(l)$ are the decay rate and diffusion coefficient of the types and $\vec{n}$ denotes nearest neighbor lattice sites. The source terms for nutrient and signal are proportional to the local concentrations of vessel-forming endothelial cells and starving tumor cells, respectively:

$$S(1) = n_1 c(4); \qquad S(2) = n_2 c(1)\Theta(b_A - b(1)), \quad (5)$$

where Θ is the Heaviside function.

Endothelial cell evolution.—In addition to the general behavior described above, ECs have additional characteristics. Migrating ECs diffuse within the tissue [the process is described similarly to Eq. (4)]. Also, migrating cells transform into closed tubes at a constant rate R_{ft}:

$$c(5) = c(5)(1 - R_{ft}), \qquad c(6) = c(6) + R_{ft}c(5). \quad (6)$$

Once they connect with preexisting vessels, closed tubes become vessels if the local concentration of $c(6)$ is larger than a threshold Q:

$$\begin{aligned} c(6) &= c(6)[1 - R_{tv}\Theta(c(6) - Q)], \\ c(4) &= c(4) + R_{tv}c(6)\Theta(c(6) - Q). \end{aligned} \quad (7)$$

Internal energy is also redistributed [13].

Pressure effects and competition for space.—Because of proliferation, the number of cells at each lattice site increases with time. Since the available space is constant, cells deform and local stress appears [16,17]. We assume the stress to be uniformly distributed within the grid element, i.e., each cell feels a stress:

$$\sigma = S(l)\frac{\tilde{d}(l) - d(l)}{\tilde{d}(l)} \quad \forall\ l, \quad (8)$$

where $S(l)$ is the elastic constant of the l type and $\tilde{d}(l) = \min[d(l), \text{Volume}/\sum_l c(l)\tilde{d}(l)]$ and $d(l)$ are the deformed and normal volumes of the l type. Stressed cells relax to equilibrium with their neighbors ($\sigma_{\vec{i}} = \sigma_{\vec{n}}$). As a consequence, an amount of cells extrudes from the stressed elements towards a less stressed nearest neighbor. Details of the calculation are reported in Ref. [18].

The model presented thus far is not exhaustive of the full set of mechanisms involved. Nevertheless, the equations described allow a reasonable first approximation description. Furthermore, the method is flexible enough to allow one to introduce in a next step some of the mechanisms neglected here, such as the influence of pressure on cell mitosis, the increased permeability of vessels when TAFs are present, and cancer cell diffusion (and metastasis) due to the reduction of cell adhesion.

Results and discussion.—We consider a square slab of tissue (40 mm^2) and discretize it as a 100×100 grid. Assuming cells with dimension of the order of 50 μm^2, in normal conditions any element can host about 800 cells (a number large enough to justify our approach). Two vessels are located at the lower corners of the specimen (see the upper right plot of Fig. 1). A tumor seed is located at ($i = 50, j = 60$) and healthy cells occupy the remaining tissue. We adopt rigid boundary conditions (bc's) for mass transport, and absorbing bc's for TAF with a constant (low) flux Φ of nutrient from boundaries into the tissue to simulate sources outside the specimen. The initial nutrient distribution corresponds to the stationary

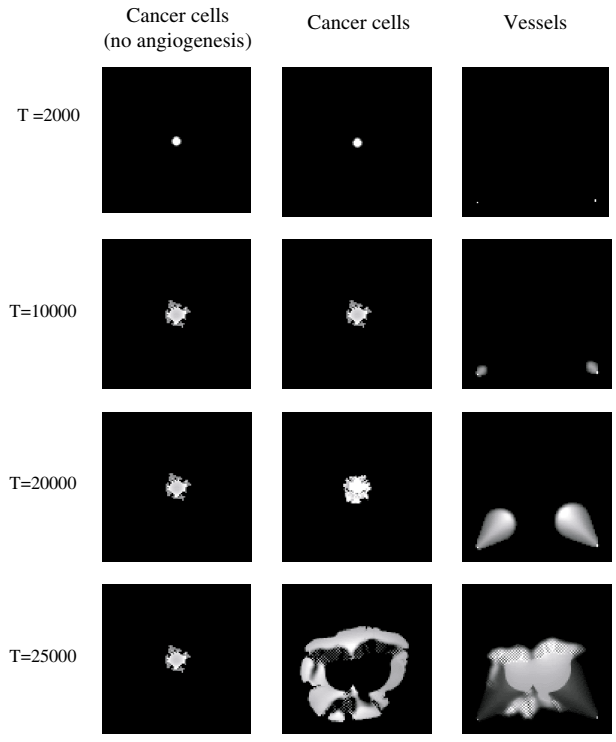

FIG. 1. Snapshots of the cancer cell and vessel concentrations during angiogenesis. Note that the ECs separation from the original vessels is apparent due to the gray scale adopted.

solutions in the absence of cancer cells. For a doubling time of about 10 h (reasonable for most tumors), the time step in the simulations corresponds to about 0.2 h.

Figure 1 shows snapshots of the concentration of cancer cells and vessels (lighter tones denote higher concentrations) at different times. Without angiogenesis, the tumor grows almost spherically until $t \sim 10\,000$, reaching a volume of about 22 mm^3, agreeing with general experimental observations. Later it remains quiescent. However, just before reaching quiescence, vascularization begins and by $t \sim 10\,000$ a few new vessels appear, though they do not yet affect tumor evolution. Later, the neoplasm resumes its growth, first slowly and then very rapidly (between $t = 20\,000$ and $t = 25\,000$), losing completely its spherical symmetry. At the same time, the neovascular system increases dramatically, with a markedly larger concentration of vessels close to the tumor edge. When (see snapshot at $t = 25\,000$ in Fig. 1) vessels infiltrate the tumor (in agreement with clinical observations), the tumor is fully vascular. The predicted profiles, not reported here for brevity, are very similar to the ones obtained in the case in which the tumor is considered stationary [13]. They present an approximate Gaussian shape with maximum located close to the tumor front, in qualitative agreement with measured microvessel densities for lung carcinomas [4].

An intense activity has been devoted in the past few years to the development of antiangiogenic drugs. Most of them are directed to target the very beginning of the vascularization process, by inhibiting ECs proliferation and migration using monoclonal antibodies which block TAF receptors. Examples are drugs which target the VEGFR2 [3,5], one of the receptors for the vascular endothelial growth factor (VEGF) [19]. On the other hand, complementary strategies have been developed to target other stages of angiogenesis: The formation of tubular structures may be reduced through metalloproteinase inhibitors [20] or the functions and survival of immature vessels (preliminary to a fully organized vascular system) may be influenced by specific compounds, such as endostatin [21].

Despite the initial enthusiasm, recent studies and clinical trials have provided disappointing results. The partial failure at a long range may be ascribed to several issues: development of drug resistance, strong sensitivity to the therapeutical protocol and schedule, interplay of the various components of the process (e.g., different mechanisms activate the same function), etc. [22]. Nevertheless, the potential for a better understanding and optimization is not diminished and therapeutic synergy between drugs targeting different stages in the vascular evolution [20,23] or with radiotherapy [24] may be crucial for the development of effective anticancer therapies.

We have simulated the action of different drugs from the literature. First, we simulate a therapeutic protocol acting on VEGFR2. Brekken and co-workers [5] have recently shown that the monoclonal antibody 2C3 blocks VEGF binding to VEGFR2, without affecting the expression of the other VEGF receptor (VEGFR1). In their experiment, they have analyzed the effects of administration of 2C3 on the growth of A673 rhabdomyosarcomas transplanted in mice. The experimental protocol consisted in repeated drug administrations (twice or 3 times per week) for about 25 d after implantation. The tumor volume was evaluated for different mice sets, treated with different drug doses (0, 1, 10, and 100 μg per injection). They reported evidence for the effect of 2C3 on VEGF binding (reduction of bound VEGF to about 25% for doses of 100 μg). The protocol may be simulated in our approach by modulating the value of ζ (assumed for simplicity to be the same for all ECs) as a function of the drug dose (assuming we know the dose-receptor inhibition relationship). In Fig. 2, we plot the volume of the tumor 25 simulated days after implantation of a single cell: in absence of therapy (taking $\zeta = 0.3$ as "normal" value), or with therapeutic administration of 2C3 at different doses: $\zeta = 0.2$ and 0.1. The drug reduces ($\zeta = 0.2$) or even completely inhibits ($\zeta = 0.1$) the growth. On the other hand, the volume becomes very large applying a drug which stimulates VEGF receptors, such as the 3E7 antibody ($\zeta = 0.4$). The results are in good quantitative agreement with the experimental findings reported in Fig. 2(b) (data taken from Fig. 5b of Ref. [5]). Remarkably, our model also predicts inhibition of angiogenesis when VEGFR2 is upregulated, in agreement with experimental findings [25]. Preliminary results, which will be reported in a forthcoming paper, seem to point out that a therapy aiming to improve VEGFR2 is more "stable," i.e., less sensitive to therapy protocol and external conditions.

Other drugs act directly on endothelial cell survival or mitotic properties, e.g., endostatin [21], which kills immature vessels [26]. For simplicity, we model *ad hoc* the action of endostatin assuming that, during the time interval of action of the drug, vessels forming ECs die at a constant rate wherever their concentration is below a critical density (assumed to be the minimal density to

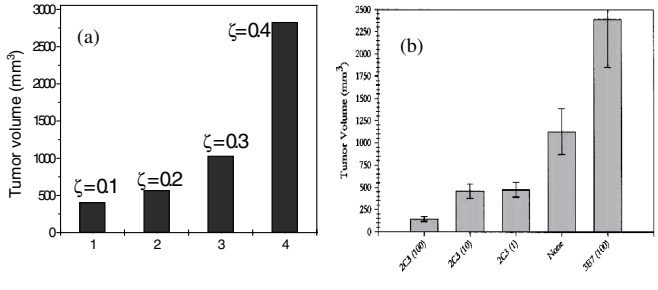

FIG. 2. (a) Final volume of the neoplasm after $T = 25\,000$ time steps for different values of ζ. (b) shows experimental data [Fig. 5b taken from Ref. [5]]. Drug doses are expressed in μg per application.

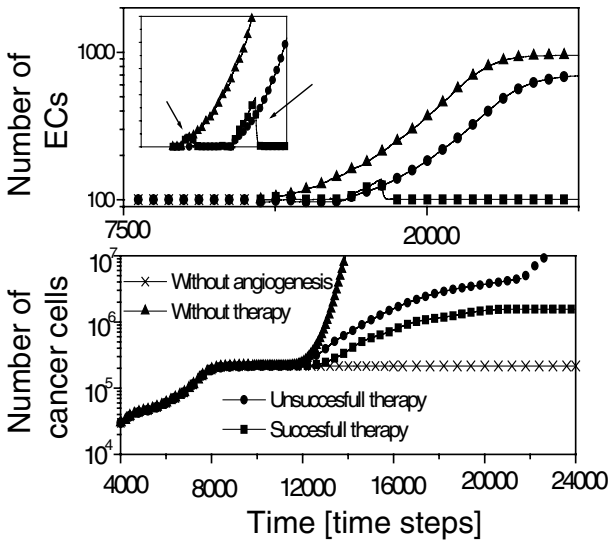

FIG. 3. Temporal evolution of the number of endothelial and cancer cells with and without angiogenesis and under two therapeutic protocols based on endostatin. In the inset of the upper plot, the arrows mark the times of drug administration.

guarantee vessels maturity). In protocol A, a single drug dose is applied in the time interval $14\,000 < t < 15\,000$; in protocol B, the therapy is applied twice: for $14\,000 < t < 15\,000$ and $16\,000 < t < 17000$. In Fig. 3, we plot the temporal evolution of the density of ECs (upper plot) and cancer cells (lower plot) in absence of angiogenesis, without therapy and with protocols A and B. In the three cases with angiogenesis, the tumor becomes larger. In the absence of therapy, the growth is very fast and uncontrolled. It is slower under protocol A and successive drug applications may even drive the tumor into a quiescent state (protocol B). Tumor growth may, however, resume at later times. The inset of the upper plot shows the drug's effect on ECs (with drug applications marked by an arrow). The results agree qualitatively with experimental data of Folkman and co-workers [27,28].

Although a more detailed link to biological mechanisms and a stronger correlation to measurable and observable parameters and quantities is desirable, the current simulation already can replicate experimental tumor response to therapy. The large number of parameters in the model is an unavoidable drawback. Nevertheless, most of the parameters (or at least several relations among them) may be directly connected to biological and observable quantities, such as the duplication time, the rate of VEGF production, etc. Although difficult to extract reliable values from the existing literature, it is possible to suggest *in vitro* experiments, or even single cell measurements (such as cantilever based measurement of elasticity), to evaluate them.

The authors thank P. P. Delsanto and G. P. Pescarmona (Torino) and C. A. Condat (Puerto Rico) for many enlightening discussions. This work was supported by the INFM Parallel Computing Initiative and by the Compagnia di San Paolo.

[1] T. Boehm *et al.*, Nature (London) **390**, 404 (1997); R. S. Kerbel, Nature (London) **390**, 335 (1997).
[2] D. Hanahan and J. Folkman, Cell **86**, 353 (1996).
[3] J. M. Wood *et al.*, Cancer Res. **60**, 2178 (2000).
[4] M. I. Koukourakis *et al.*, Cancer Res. **60**, 3088 (2000).
[5] R. A. Brekken *et al.*, Cancer Res. **60**, 5117 (2000).
[6] A. Brù *et al.*, Phys. Rev. Lett. **81**, 4008 (1998).
[7] S. C. Ferreira *et al.*, Physica (Amsterdam) **272A**, 245 (1999).
[8] M. Scalerandi *et al.*, Phys. Rev. E **59**, 2206 (1999); Phys. Rev. E **62**, 2547 (2000); J. Surg. Oncol. **74**, 122 (2000).
[9] H. M. Byrne, J. Math. Biol. **39**, 59 (1999).
[10] E. Stott *et al.*, Math. Comput. Model. **30**, 183 (1999).
[11] A. R. Kansal *et al.*, J. Theor. Biol. **203**, 367 (2000).
[12] M. J. Holmes *et al.*, J. Theor. Biol. **202**, 95 (2000).
[13] B. Capogrosso Sansone *et al.*, Phys. Rev. Lett. **87**, 128102 (2001); Phys. Rev. E **65**, 011902 (2002).
[14] J. C. M. Mombach and J. Glazier, Phys. Rev. Lett. **76**, 3032 (1996).
[15] T. Hofer *et al.*, Physica (Amsterdam) **85D**, 425 (1995).
[16] A. J. Perumpanani *et al.*, Physica (Amsterdam) **126D**, 145 (1999).
[17] B. Capogrosso Sansone *et al.*, Phys. Rev. E **64**, 021903 (2001).
[18] M. Scalerandi *et al.*, Phys. Rev. E **65**, 051918 (2002).
[19] M. Asano *et al.*, Hybridoma **17**, 185 (1998); S. Mesiano *et al.*, Am. J. Clin. Pathol. **153**, 1249 (1998); M. Skobe *et al.*, Nature Medicine **3**, 1222 (1997); M. Prewett *et al.*, Cancer Res. **59**, 5209 (1999).
[20] G. Bergers *et al.*, Science **284**, 808 (1999).
[21] P. Blezinger *et al.*, Nature Biotechnol. **17**, 343 (1999).
[22] P. Carmeliet and R. K. Jain, Nature (London) **407**, 249 (2000).
[23] R. Cao *et al.*, Proc. Natl. Acad. Sci. U.S.A. **96**, 5728 (1999).
[24] H. J. Mauceri *et al.*, Nature (London) **394**, 287 (1998).
[25] T. Masazaku *et al.*, LANCET Oncol. **2**, 667 (2002), and references therein.
[26] T. Bohem *et al.*, Cell **88**, 277 (1997).
[27] G. Perletti *et al.*, Cancer Res. **60**, 1773 (2000).
[28] M. S. O'Reilly *et al.*, Nature Medicine **2**, 689 (1996).